ACS NANO

www.acsnano.org

ARTICLE

Epitaxial Synthesis of Highly Oriented 2D Janus Rashba Semiconductor BiTeCl and BiTeBr Layers

Debarati Hajra, Renee Sailus, Mark Blei, Kentaro Yumigeta, Yuxia Shen, and Sefaattin Tongay*

Cite This: *ACS Nano* 2020, 14, 15626−15632

Read Online

ACCESS | Metrics & More | Article Recommendations | SI Supporting Information

ABSTRACT: **The family of layered BiTeX (X = Cl, Br, I) compounds are intrinsic Janus semiconductors with giant Rashba-splitting and many exotic surface and bulk physical properties. To date, studies on these materials required mechanical exfoliation from bulk crystals which yielded thick sheets in nonscalable sizes. Here, we report epitaxial synthesis of Janus BiTeCl and BiTeBr sheets through a nanoconversion technique that can produce few triple layers of Rashba semiconductors (<10 nm) on sapphire substrates. The process starts with van der Waals epitaxy of Bi_2Te_3 sheets on sapphire and converts these sheets to BiTeCl or BiTeBr layers at high temperatures in the presence of chemically reactive $BiCl_3$/$BiBr_3$ inorganic vapor. Systematic Raman, XRD, SEM, EDX, and other studies show that highly crystalline BiTeCl and BiTeBr sheets can be produced on demand. Atomic level growth mechanism is also proposed and discussed to offer further insights into growth process steps. Overall, this work marks the direct deposition of 2D Janus Rashba materials and offers pathways to synthesize other Janus compounds belonging to MXY family members.**

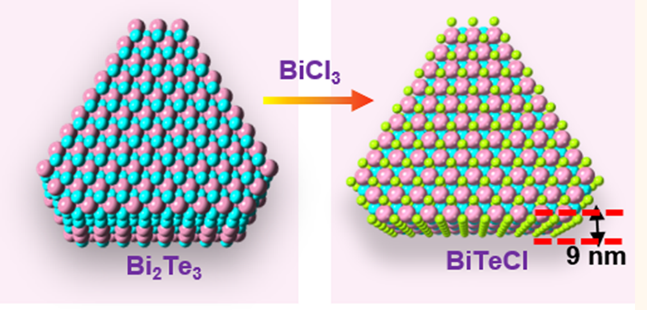

KEYWORDS: *Janus, epitaxy, inversion-symmetry, van der Waals gap, bismuth tellurohalide, Raman spectroscopy*

Bismuth telluro chloride (BiTeCl), a recently discovered inversion-asymmetric topological insulator (TI)[1] is a member of the family of noncentrosymmetric Janus Rashba-semiconductors BiTeX (X = Cl, Br, I), which have recently generated a strong interest due to their versatile quantum phases.[1−9] This family of layered materials features intrinsic "*Janus*"[2,3] sublayers consisting of individual layers of metal, halogen, and chalcogen atoms stacked together in triple-layers (TLs), separated along the hexagonal *c*-axis of the crystal by a weak van der Waals (vdW) force (Figure 1a−d). This special atomic arrangement induces charge-separation along the stacking direction and large built-in electric field within each Janus layer.[1,4] Similar to other BiTeX materials, heavy Bi atom-induced spin−orbit coupling (SOC) and lack of inversion symmetry lifts the spin degeneracy in the bulk and surface electronic states of BiTeCl causing spin-polarized "Rashba" states[1−5] as predicted in theoretical models,[6] and experimentally confirmed by angle-resolved photoemission spectroscopy (ARPES).[4,6]

Rashba splitting makes BiTeCl and BiTeBr a strong candidate for use in spintronics.[1,5] For example BiTeCl is a narrow-gap semiconductor ($E_g \sim 0.8$ eV)[6] which has been demonstrated to have *n*-type and *p*-type surface states for Te and Cl terminated exfoliated flakes.[6] So far BiTeCl/BiTeBr are the only strong-inversion-asymmetric TI, with the only other candidate being HgTe with weak inversion asymmetry.[10] Interestingly, superconductivity is shown to exist in BiTeCl at pressures above 5 GPa[11] which is rarely observed in TIs. These properties in one layered material make Janus Rashba-semiconductors BiTeX a promising candidate for spintronic and optoelectronic applications and offer opportunities to study the interplay of contrasting quantum phenomena coexisting in a single material.

Previous electronic transport studies on Janus Rashba BiTeX have been mostly carried out on samples mechanically exfoliated from bulk crystals[12,13] grown by topotactic method.[14] Although this technique can transfer highly crystalline samples, only samples of nonscalable size (both

Received: July 31, 2020
Accepted: October 16, 2020
Published: October 22, 2020

https://dx.doi.org/10.1021/acsnano.0c06434
ACS Nano 2020, 14, 15626−15632

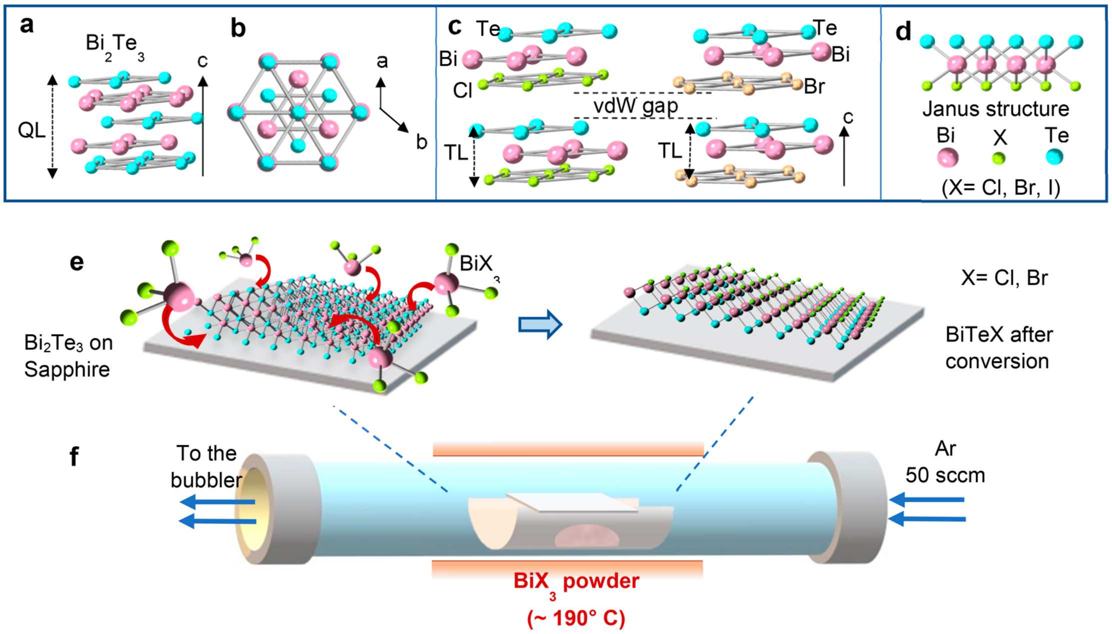

Figure 1. Overviews of triple-layer (TL) in Janus BiTiX (X = Cl, Br, and I) and schematic of their epitaxial synthesis. a,b. Hexagonal crystal structure of one quintuple layer (QL) Bi_2Te_3 and c. noncentrosymmetric Janus structure of BiTeCl and BiTeBr. d. Triple-layer structure of BiTeX family showing two different faces of a single Janus layer. e. Schematic outline of the conversion processand f. implemented experimental setup for conversion process of Bi_2Te_3 into BiTeCl or BiTeBr.

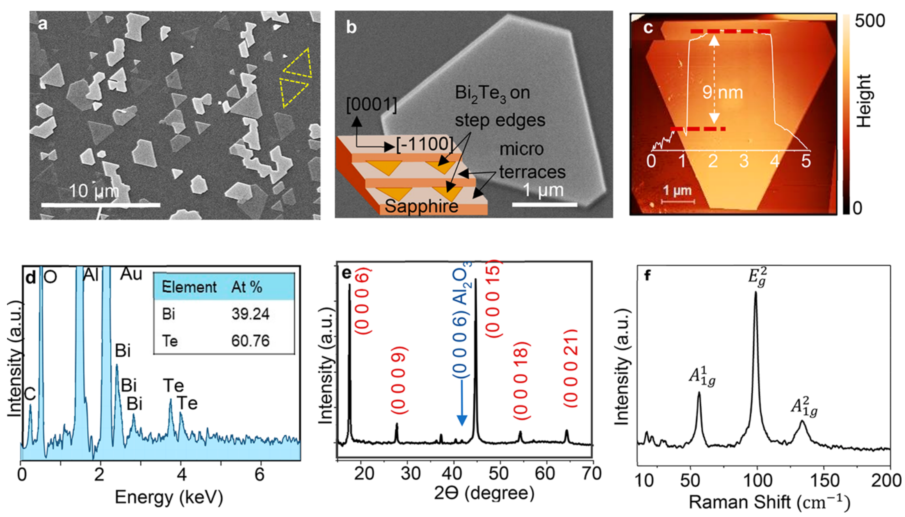

Figure 2. a. Low magnification SEM image of Bi_2Te_3 sheets. Two common orientations of Bi_2Te_3 flakes shown by dashed yellow lines. b. High magnification SEM image of single Bi_2Te_3 nanosheet; The inset shows orientation of the triangular nanosheets with respect to single crystal sapphire substrate on the terraces. c. Atomic force microscopy image of a typical Bi_2Te_3 flake and AFM line scan plot highlighting its height profile. d. Energy dispersive X-ray (EDX) analysis showing 2:3 stoichiometry of Bi_2Te_3 sheets. e. XRD data collected from Bi_2Te_3 nanosheets showing high crystallinity and orientation. f. Raman spectra of Bi_2Te_3 with all vibrational modes.

thickness and lateral size) can be accessed without any substrate orientation control. No thin-film BiTeCl or other Bi based Janus layered growth has been reported to date through bottom-up and scalable epitaxial method.

Here, we report the synthesis of ultrathin BiTeCl and BiTeBr sheets by conversion of Bi_2Te_3 sheets into BiTeX (X = Cl, Br) in the presence of BiX_3 vapor. The method produces flakes as thin as <10 nm with excellent elemental uniformity and crystalline characteristics as confirmed by a variety of characterization techniques. We further offer a possible growth mechanism to explain the conversion process and atomic level chemical reaction to establish the foundations of this type of growth process. Overall, this work enables a time- and cost-effective growth method for producing Bi based Janus crystals (BiTeX, X = Br or Cl) and offers the opportunity to investigate atomic-level phenomena not previously studied due to the limitations imposed by film thickness.

RESULTS AND DISCUSSION

Topological Bi_2Te_3 vs. Janus BiTeCl vdW layers. Figure 1a–d depicts the crystal structures of Bi_2Te_3 and Janus BiTeX (X = Cl, Br, I). The parent material, Bi_2Te_3, crystallizes in a hexagonal structure with $R\bar{3}m$ spacegroup whereas non-centrosymmetric BiTeCl and BiTeBr belong to hexagonal

P6₃mc and *P3m1* space groups, respectively. One unit cell of Bi_2Te_3 contains three quintuple layers (QL) of Te−Bi−Te−Bi-Te stacked together along the *c*-axis.[15] Compared to Bi_2Te_3, one unit cell of BiTeX (X = Cl, Br) consists of two(one) triple-layers(TL) of Te−Bi-X sandwich, with a vdW gap between two adjacent TLs perpendicular to the *c*-axis.[13,18] In each TL, Bi−Te and Bi−Cl are bonded covalently while Te-X bonds across the vdW gap are bonded by much weaker vdW forces. Because each Te−Bi-X triple-layer contains different faces (Te vs. X), BiTeX crystals are often referred to as Janus crystals, named after the two-faced Roman God Janus. Here, it is important to note that Bi_2Te_3 and BiTeX have a strongly similar crystal symmetry; possibly one of the factors to promote the conversion process which will be discussed later in the article.

Synthesis Process. Our method starts with the CVD deposition of ultrathin (∼5−10 nm) Bi_2Te_3 sheets onto *c*-cut sapphire substrates. In a typical growth process, Bi_2Te_3 sheets were synthesized using Bi_2Te_3 powder as a precursor in a 1 in. diameter quartz tube furnace by vdW epitaxy using established protocols in the literature.[16] Bi_2Te_3 powder was kept at 480 °C while target substrates were at 12 cm downstream from the center where the temperature was 200 °C. Prior to the deposition step, (0001) cut sapphire substrates were preannealed at 1850 °C in the presence of Argon gas to introduce atomically flat terraces with step edges along the [−1100] direction (shown in inset of Figure 2b). We find that introducing these sharp steps is helpful in facilitating the nucleation process along the chemically active (lower nucleation barrier) step-edges (for details see the Methods section).

After the growth, mostly truncated triangles of lateral size ∼5 μm and few QL thickness measuring ∼8−9 nm[16] were obtained along (0001) orientation as shown in the SEM and AFM scan images (Figure 2a−c). Raman microscopy, XRD, and EDX characterizations confirmed the composition and crystallinity of Bi_2Te_3 QL sheets as shown in Figure 2d−f. XRD scans mainly yield {000*l*} reflections, confirming the layer-by-layer growth mode which produces well-aligned Bi_2Te_3 sheets. The three most prominent Bi_2Te_3Raman peaks were observed at 56 cm^{-1}, 99 cm^{-1}, and 134 cm^{-1} consistent with the literature.[17] These peaks had narrow full widths at half-maximum (fwhm) (∼3, 4, and 6 cm^{-1}, respectively) further confirm the high crystallinity of Bi_2Te_3 QLs. One important observation is that Bi_2Te_3 triangle sheets have two possible orientations with respect to the sapphire substrate, which is shown with dashed outline in Figure 2a. One of the edges of the triangles is parallel to the [−1100] direction of the sapphire substrate (Figure 2b inset). Hexagonal symmetry of [0001] oriented sapphire ultimately guides the growth of hexagonal Bi_2Te_3 with these specific orientations, also observed by other researchers in this field.[19]

Conversion through Solid−gas Reaction. Conversion of Bi_2Te_3 into BiTeCl was carried out in a one-inch diameter quartz tube placed inside a one-zone furnace as schematically shown in Figure 1f. In the big picture, the conversion relies on chemical reaction between Bi_2Te_3 vdW sheets with chemically reactive $BiCl_3$ vapor to form BiTeCl layers (the transformation process details are offered later in the article). To accomplish that, $BiCl_3$ powder was placed in an alumina boat kept at the center of the furnace and Bi_2Te_3/sapphire substrates were placed face down above the alumina boat directly facing the $BiCl_3$ vapor/precursor. To maintain a nonreactive environment (i.e., to prevent oxidation of Bi_2Te_3) and to prevent excess $BiCl_3$ vapor pressure, Ar flow of 50 sccm was maintained during the experiment. Without the Ar flow, Bi_2Te_3 sheets reacted with ambient oxygen and produced thin layer of tellurium oxide (TeO_x) on the surface which significantly impeded the conversion process.

Our comprehensive studies have shown that growth temperature range and duration ultimately dictate a successful Janus conversion process. For example, any growth at temperatures above 210 °C caused Bi_2Te_3 ultrathin sheets to deteriorate by decomposition process due to the low melting point of Bi_2Te_3. Also, growth temperatures below 180 °C were not sufficient for sublimation of $BiCl_3$ ($T_{melting}$ ∼ 230 °C) and thus prevented the Janus conversion process. Considering the material stability and precursor sublimation, the conversion process only offered very narrow 180 °C < T_g < 210 °C growth temperature range. Even when the temperature range is finely tuned, for longer conversion times (>6 min) most of the thin films suffered major surface degradation, while shorter conversion times resulted in partially converted Janus BiTeCl sheets. In our studies, the optimal growth parameter was 190 °C source zone temperature with 5 min growth duration.

To confirm the presence of BiTeCl sheets, we have used conventional nondestructive Raman spectroscopy. Previously, this method has been widely used to characterize bulk BiTeCl[12,13,20] as well as other Janus crystals with well-established Raman spectra. Vibrational representation of zone-center phonons of BiTeCl can be written as $\Gamma = 2A_1+3B_1+2E_1+2E_2$ where all the modes should be observed except silent B_1 modes. After the conversion process, we find that previously established Bi_2Te_3 Raman peaks at 56, 99, and 134 cm^{-1} disappear and new peaks emerge (Figure 3a) at 82, 97, 118, 119, 138, and 152 cm^{-1} which correspond to E_2^2,E_2^1,E_{1g}^1,E_1^2,A^2 and A_1^1 modes, respectively. The rigid layer mode E_2^3 was found at 18 cm^{-1}. We note that while these peaks are located at correct positions, their relative intensities with respect to each other can be different across bulk and thin-film Janus layers (Supporting Information (SI) Figure S2).[13] Previously similar thickness induced trends were shown for other vdW materials including $MoTe_2$,[21,22] WSe_2,[23] and

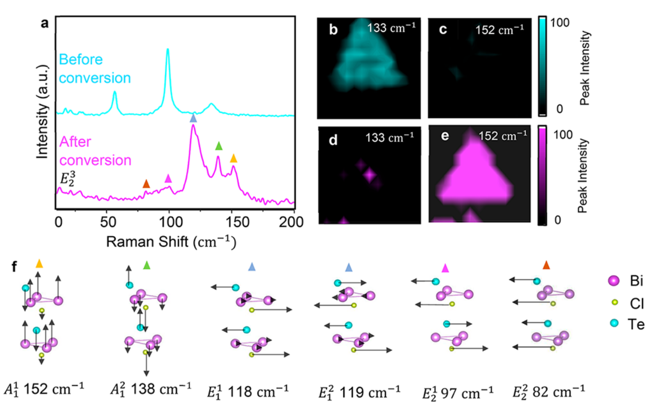

Figure 3. a. Raman Spectra of parent (Bi_2Te_3) and product (BiTeCl) sheets before and after conversion. b,d. Raman mapping of mode A_{1g}^2 at 133 cm^{-1} in Bi_2Te_3 before and after conversion, respectively. c,e. Raman mapping of A_1^1 mode at 152 cm^{-1} of BiTeCl before and after conversion, respectively, indicating uniform conversion. f. atomic displacements corresponding to different vibrational modes of BiTeCl.

others[24] and is likely related to changes in Raman scattering cross-section with respect to material thickness.

Uniformity Across the Flake and Stability. To assess the uniformity of the conversion process, we provide the Raman mapping data of two different flakes before and after conversion, as seen in Figure 3b−e. Figure 3b,d show the peak intensity plot of A_{1g}^2 mode for Bi_2Te_3 before and after conversion, respectively. As expected, the peak intensity is uniform throughout the sample before conversion and is absent in the sample after conversion. In Figure 3c,e, we show a similar map at BiTeCl A_1^1 mode before and after conversion. The peak intensity is uniformly distributed over the sample area after conversion, confirming the uniform and complete conversion of Bi_2Te_3 nanosheets into BiTeCl. EDX mapping of elements Bi, Te, and Cl in Figure 4a−d also confirms uniformity in distribution of all three elemental components of BiTeCl.

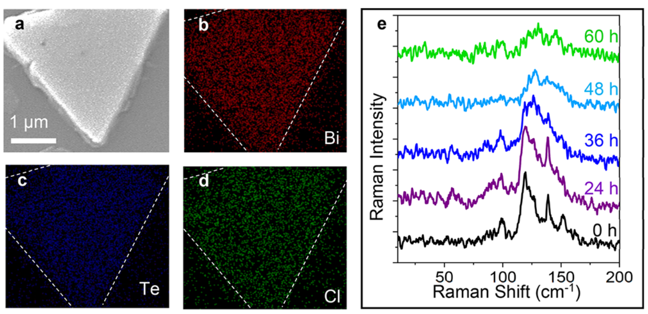

Figure 4. a−d. Elemental composition mapping by SEM-EDX on synthesized BiTeCl ultrathin sheets showing individual contribution of Bi, Te, and Cl. e. Degradation of vibrational response of BiTeCl thin films as observed by Raman spectra taken at several time intervals after exposure to ambient air.

Typically, CVD or PVD grown 2D or vdW materials have been shown to be more prone to environmental degradation effects[25] and chalcogen vacancies have been suggested as one of the primary reasons for metastability. To understand the stability of the synthesized BiTeCl vdW sheets, we performed time dependent Raman spectroscopy to study the change in vibrational properties after exposing the thin films in ambient air (Figure 4e). Measurement at 0 h refers to Raman spectra collected immediately after the conversion process and samples were kept in ambient conditions (air and 20 °C) for a prolonged amount of time up to 60 h. In the first 24 h time frame, the Raman spectra had shown no noticeable changes but started to broaden and produce weaker signals beyond 24 h. This can be attributed to an increased number of defects in the material and deviation from $\Gamma = 0$ Raman condition whether the defect originates from oxidization or the material degradation process. Prior studies have also shown similar degradation effects on other Te based material systems including GaTe, $ZrTe_3$,[26,27] tellurene,[28,29] and others.[30,31] These researches show that, reaction with O_2 and H_2O can be detrimental to tellurium-based thin films. Interplay of multiple degradation mechanisms, for example. adsorption of gaseous molecules (O_2, H_2O, NO_2, NH_3, H_2S, *etc.*) from air followed by their dissociation in the presence of vacancies is highly probable. A possible reaction route enhancing surface degradation canbe $BiTeX + H_2O = BiTe_{(1-y)}X + Te_yO_x +$ biproducts. Our results suggest that synthesized few layer thick BiTeCl sheets must be either be protected by surface functionalization,[27] encapsulated with other 2D sheets(for example. few layers h-BN)[32,33] *etc.* or kept under inert gas conditions for increased self-life.

Applicability to other BiTeX Rashba Layers. To investigate the applicability of this technique for growth of materials within the same family, we attempted conversion of BiTeBr and BiTeI in the presence of $BiBr_3$ and BiI_3 vapor, respectively, from PVD-grown Bi_2Te_3. The conversion of BiTeBr was carried out using a similar experimental setup with the center of the furnace set to 180 °C ($T_{melting}$ of $BiBr_3 \sim 220$ °C). Raman spectra (Figure 5a−c) taken after the conversion process indicates the presence of BiTeBr. Raman mapping in mode A_1 presented in Figure 5b shows near uniform conversion.

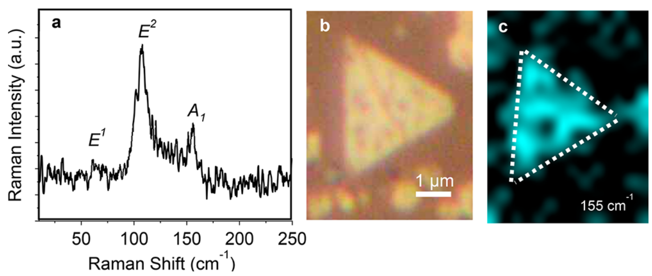

Figure 5. a. Raman spectra of BiTeBr nanosheet after conversion. b. Optical image. c. Raman peak intensity mapping for the BiTeBr A_1 mode at 155 cm^{-1} demonstrating nearly uniform conversion.

Due to higher temperature requirements, the experimental setup was modified for converting BiTeI, in which the center of the furnace was held at 350 °C to allow sublimation of BiI_3($T_{melting}$ of $BiI_3 \sim 400$ °C). The sapphire substrate with the Bi_2Te_3 thin film was placed on a separate Al_2O_3 boat 10 cm downstream of the furnace center to avoid damaging the film, in a zone of ∼180 °C. This setup did not result in conversion, as BiI_3 recrystallizes in the temperature zone 150−250 °C.

We further attempted the growth of SbTeCl and SbTeBr by the same method (S4) where the conversion process did not take place (SI Figure S4). To the best of our knowledge, crystal structures of SbTeCl(Br) are not experimentally established at the time of writing and SbTeI does not belong to Janus family.[34] Lack of similarity between the parent (Sb_2Te_3) and the product (SbTeX) can be a possible reason for this as we mention in the growth mechanism section.

Growth Mechanism. Here, we present one possible growth mechanism that can account for the Bi_2Te_3 conversion into BiTeX, as few striking structural similarities between these two layered materials can facilitate the conversion process. The crystal structure of both materials consists of individual planes of all the elements (Bi, Te for Bi_2Te_3 and Bi, Te, X for BiTeX). A closer look at the crystal structure of Bi_2Te_3 reveals that the coordination octahedra of Bi atoms consists of six Te atoms which are similar to the coordination octahedra of Bi atoms in BiTeX with the top three Te atoms replaced by X atoms (Figure 6a,b). Bi−Te bond lengths are also close in both materials (3.10−3.29 Å in Bi_2Te_3 and 3.05 and 3.06 Å in BiTeCl and BiTeBr, respectively). These atomic-level structural similarities are suggestive of an energetically favorable conversion process from Bi_2Te_3 to BiTeX.

We first emphasize that if Bi_2Te_3 flakes measure thicker than 10 nm these sheets can only be partially converted to BiTeX, but thinner flakes (<10 nm) can easily undergo a full

https://dx.doi.org/10.1021/acsnano.0c06434
ACS Nano 2020, 14, 15626−15632

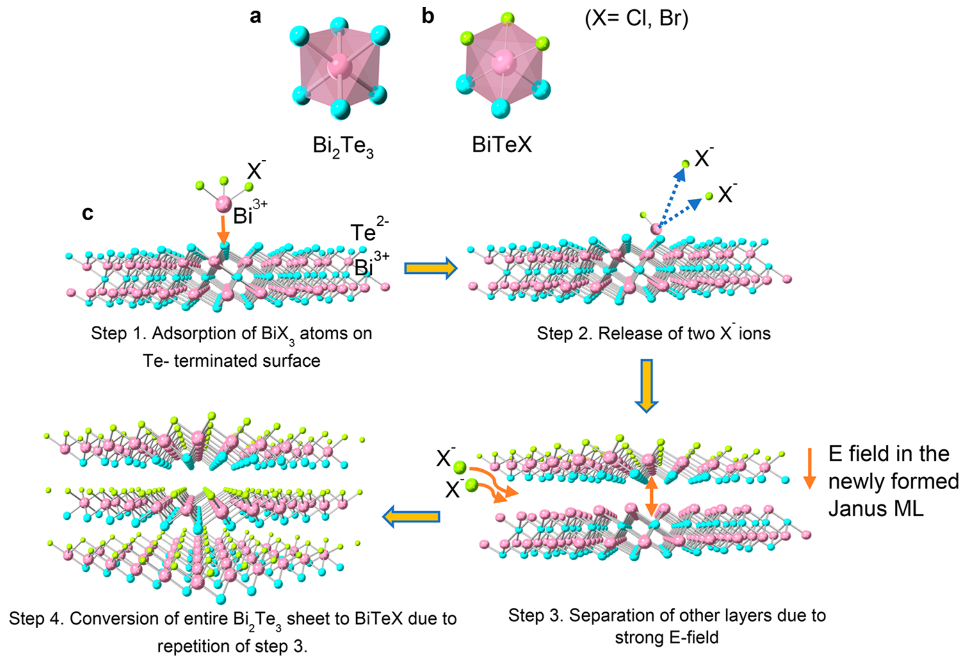

Figure 6. a,b. Similarity between coordination octahedra in Bi_2Te_3 and BiTeX (X = Cl, Br), suggestive of the feasibility of conversion from Bi_2Te_3 and BiTeX. c. Possible steps of the conversion process: Step 1, attraction of Bi^{3+} ions of BiX_3 toward Te^{2-} of Bi_2Te_3; Step 2, release of two X^- ions from BiX_3 to maintain neutral charge with the Te layer; Step 3, formation of first BiTeX Janus layer with a high E-field toward the Te-plane which causes adjacent bottom layers to be separated. Intercalation of X^- ions in the newly formed vdW gap converts next layers into BiTeX; Step 4, conversion of entire Bi_2Te_3 sheet due to repetition of Step 3.

conversion. We also note that conversion process does not start from the edges of Bi_2Te_3 since halting the growth process without reaching full conversion does not yield BiTeX at the edge sites. These observations indicate the conversion process starts at the surface of the Bi_2Te_3 flakes and gradually proceeds toward bottom layers.

The atomic mechanism of the conversion process is depicted in detail in Figure 6. First, BiX_3 powder sublimes and goes into gaseous phase $BiX_3(g)$ which in turn reacts with the top surface of Bi_2Te_3. Being an ionic compound, $BiCl_3$ shares its total charge as Bi^{3+} and $3X^-$, while Te terminated Bi_2Te_3 has a surface charge of Te^{2-}. First, Bi^{3+} of a BiX_3 molecule reacts with Te^{2-} terminated surface due to high local partial gas pressure of BiX_3. We argue that two X^- ions from BiX_3 are released to maintain charge neutrality with Te^{2-} layers. This forms the first "nucleation site" of BiTeCl, and the process repeats to form the first layer of BiTeX on the surface after rearrangement of the Te atoms into new energetically favorable positions. Once the first layer of BiTeX is formed, a strong electric field (polarization field) directed toward the Te layer develops within the Janus layer. This electric field separates adjacent layers having a net positive charge along the *c*-axis, creating a vdW gap as observed in various DFT studies. Extra X^- species diffuse through the vdW gap *via* intercalation to form the next BiTeCl layers. Each time a new Janus layer forms, it creates a separation with the adjacent layers until the whole Bi_2Te_3 flake converts into BiTeX. This process is particularly successful for thin sheets (<10 nm) since the number of layers is limited and thus the process time is short. In contrast, thicker sheets require longer conversion time and results in partially converted sheets. To avoid surface degradation of the nanosheets (mentioned earlier), we did not raise the conversion time above 7 min, which was insufficient to fully convert thicker (>10 nm) flakes. Another potential growth mechanism might be phase transformation of $Bi_2Te_3 \rightarrow BiTe$ by chalcogen defect generation at growth temperatures, followed by BiTe → BiTeCl transformation similar to the process described above. To test this potential route, we have annealed Bi_2Te_3 nanosheets under the same experimental conditions except without the $BiCl_3$ powder. Comprehensive Raman spectra collected on Bi_2Te_3 sheets-(S5)show no significant changes before and after the annealing process which precludes the possibility of an intermediary BiTe step and makes the latter process unlikely. Although this hypothesis lays a foundation in understanding the conversion process at the trilayer level, future theoretical studies such as calculation of energy of formation at the growth temperature, DFT and charge analysis (*e.g.*, Bader charge analysis) are suggested to understand the feasibility, charge sharing mechanism during adsorption of BiX_3 and intercalation of X-species.

CONCLUSION

In summary, we have demonstrated the direct synthesis of orientation-controlled ultrathin (~15 layer thick) BiTeCl and BiTeBr Janus layers on sapphire substrates using nanoscale conversion process. These studies show the demonstration of their synthesis in ultrathin form without the need for exfoliating bulk crystals. Comprehensive measurements further confirm the quality and uniformity of these Janus BiTeCl and BiTeBr sheets. A detailed growth mechanism is offered to understand the nature of this transformation process from Bi_2Te_3 to BiTeX vdW sheets. Overall results established ways to deposit these materials in few-layer form and may offer potential ways to extend these results to other 2D Janus crystals belonging to MXY (M = Bi, Sb X = Se and Te, and X = Cl, Br, I) quantum material systems.

https://dx.doi.org/10.1021/acsnano.0c06434
ACS Nano 2020, 14, 15626−15632

METHODS

Bi_2Te_3 vdW Sheet Synthesis. Bi_2Te_3 vdW sheets were grown on c-cut sapphire by physical vapor deposition in a single-zone Lindberg tube-furnace (model TF55030A-1). A c-cut sapphire substrate was preannealed at temperature 1850 °C in Argon atmosphere for 1 h to create parallel terraces on the substrate-surface along [−1100] direction. During the growth 2 mg of Bi_2Te_3 (Alpha Aesar, 99.98%) powder was placed in a quartz boat in a one-inch diameter quartz tube at the center of the furnace (480 °C) and sapphire substrate was kept at 12 cm downstream from the center in a separate quartz boat where the temperature is ∼200 °C. Though the tube was cleaned with 200 sccm Ar prior to the experiment, no gas flow was maintained during the growth. The pressure inside the tube was maintained at 200 mTorr. The temperature was raised from room temperature to 480 °C at 20 °C/min and was kept at 480 °C for 5 min. At the end of the process the furnace was allowed to cool to room temperature naturally.

BiTeCl(Br) Conversion. BiTeCl(Br) conversion process was performed in the same furnace. Five mg of $BiCl(Br)_3$ powder (Sigma-Aldrich, 99.99% trace metal basis) was kept at the center of the furnace in an Al_2O_3 boat with Bi_2Te_3 deposited substrate above it. Temperature was raised to ∼190 (200) °C at 20 °C/min rate and Argon flow of 50 sccm was maintained during the experiment. An average growth time of ∼5 min was maintained for both materials, after which the furnace was allowed to cool to room temperature. Before beginning the conversion process the quartz tube was purged by Argon flow at 200 sccm to remove unwanted impurities. This technique has been repeated to more than 25 samples before concluding the work.

Atomic Force Microscopy. Atomic force microscopy images were acquired by NT-MDT AFM-system in semicontact mode by Silicon tips with Al-coatings.

XRD. X-ray diffraction data from Bi_2Te_3 thin films were acquired by high resolution Panalytical X'Pert Pro MRD with Cu $K_{\alpha1}$ wavelength. Fixed divergence slits were used as the incident beam optics and detection of the diffracted rays was done by X'Celerator detector.

Raman Spectroscopy. Raman spectroscopy measurements were done with a homemade Raman microscope in backscattering geometry with unpolarized 532 nm incident laser (1.3 mW) in backscattering geometry with spectral resolution 1 cm^{-1}. Scattered light intensity was measured without any analyzer at the detector. To avoid oxidation of thin films under Laser sample was kept in a vacuum chamber with quartz window at 100 mTorr during the measurement. For Raman mapping a different Renishaw spectrometer with polarized incident light of wavelength 488 nm was used with backscattering geometry.

Scanning Electron Microscopy and Energy Dispersive X-ray Spectroscopy. Scanning electron microscopy (SEM) of Bi_2Te_3 nanosheets was done with an Amray 1910 field electron scanning electron microscope at 15 keV with ∼2 nm resolution. The sapphire substrate with Bi_2Te_3 was fixed on an Al sample holder by carbon tape. Prior to SEM imaging, the substrate was coated with 20 nm gold to avoid the effect of sample charging. EDX spectra and elemental mapping were acquired with the same microscope with EDAX Octane Series Silicon Drift Detector.

ASSOCIATED CONTENT

Supporting Information

The Supporting Information is available free of charge at https://pubs.acs.org/doi/10.1021/acsnano.0c06434.

Bulk growth and characterization of BiTeCl; analysis of Raman spectra of bulk and thin film BiTeCl samples; Sb-based Janus thin-film growth; temperature treatment of Bi_2Te_3 thin films (PDF)

AUTHOR INFORMATION

Corresponding Author

Sefaattin Tongay − *Materials Science and Engineering, School for Engineering of Matter Transport of Energy, Arizona State University, Tempe, Arizona 85287, United States;* orcid.org/0000-0001-8294-984X; Email: sefaattin.tongay@asu.edu

Authors

Debarati Hajra − *Materials Science and Engineering, School for Engineering of Matter Transport of Energy and Department of Physics, Arizona State University, Tempe, Arizona 85287, United States*

Renee Sailus − *Materials Science and Engineering, School for Engineering of Matter Transport of Energy, Arizona State University, Tempe, Arizona 85287, United States*

Mark Blei − *Materials Science and Engineering, School for Engineering of Matter Transport of Energy, Arizona State University, Tempe, Arizona 85287, United States*

Kentaro Yumigeta − *Materials Science and Engineering, School for Engineering of Matter Transport of Energy and Department of Physics, Arizona State University, Tempe, Arizona 85287, United States*

Yuxia Shen − *Materials Science and Engineering, School for Engineering of Matter Transport of Energy, Arizona State University, Tempe, Arizona 85287, United States*

Complete contact information is available at: https://pubs.acs.org/10.1021/acsnano.0c06434

Notes

The authors declare no competing financial interest.

ACKNOWLEDGMENTS

We acknowledge the use of facilities within the Eyring Materials Center at Arizona State University supported in part by NNCI-ECCS-1542160. S.T acknowledges support from DOE-SC0020653, NSF CMMI 1933214, NSF DMR 1552220, and DMR 1955889.

REFERENCES

(1) Chen, Y.; Kanou, M.; Liu, Z.; Zhang, H.; Sobota, J.; Leuenberger, D.; Mo, S.; Zhou, B.; Yang, S.; Kirchmann, P. Discovery of a Single Topological Dirac Fermion in the Strong Inversion Asymmetric Compound BiTeCl. *Nat. Phys.* **2013**, *9*, 704−708.

(2) Yagmurcukardes, M.; Qin, Y.; Ozen, S.; Sayyad, M.; Peeters, F.; Tongay, S.; Sahin, H. Quantum Properties and Applications of 2D Janus Crystals and Their Superlattices. *Appl. Phys. Rev.* **2020**, *7*, 011311.

(3) Li, H.; Qin, Y.; Ko, B.; Trivedi, D. B.; Hajra, D.; Sayyad, M. Y.; Liu, L.; Shim, S. H.; Zhuang, H.; Tongay, S. Anomalous Behavior of 2D Janus Excitonic Layers under Extreme Pressures. *Adv. Mater.* **2020**, *32*, 2002401.

(4) Ma, Y.; Dai, Y.; Wei, W.; Li, X.; Huang, B. Emergence of Electric Polarity in BiTeX (X= Br and I) Monolayers and the Giant Rashba Spin Splitting. *Phys. Chem. Chem. Phys.* **2014**, *16*, 17603−17609.

(5) Crepaldi, A.; Moreschini, L.; Autes, G.; Tournier-Colletta, C.; Moser, S.; Virk, N.; Berger, H.; Bugnon, P.; Chang, Y.; Kern, K. Giant Ambipolar Rashba Effect in the Semiconductor BiTeI. *Phys. Rev. Lett.* **2012**, *109*, 096803.

(6) Landolt, G.; Eremeev, S. V.; Tereshchenko, O. E.; Muff, S.; Slomski, B.; Kokh, K. A.; Kobayashi, M.; Schmitt, T.; Strocov, V. N.; Osterwalder, J. Bulk and Surface Rashba Splitting in Single Termination BiTeCl. *New J. Phys.* **2013**, *15*, 085022.

(7) Eremeev, S. V.; Nechaev, I. A.; Koroteev, Y. M.; Echenique, P. M.; Chulkov, E. V. Ideal Two-Dimensional Electron Systems with a

Giant Rashba-Type Spin Splitting in Real Materials: Surfaces of Bismuth Tellurohalides. *Phys. Rev. Lett.* **2012**, *108*, 246802.
(8) Fiedler, S.; Bathon, T.; Eremeev, S. V.; Tereshchenko, O. E.; Kokh, K. A.; Chulkov, E. V.; Sessi, P.; Bentmann, H.; Bode, M.; Reinert, F. Termination-Dependent Surface Properties in the Giant-Rashba Semiconductors BiTeX (X= Cl, Br, I). *Phys. Rev. B: Condens. Matter Mater. Phys.* **2015**, *92*, 235430.
(9) Ishizaka, K.; Bahramy, M.; Murakawa, H.; Sakano, M.; Shimojima, T.; Sonobe, T.; Koizumi, K.; Shin, S.; Miyahara, H.; Kimura, A. Giant Rashba-Type Spin Splitting in Bulk BiTeI. *Nat. Mater.* **2011**, *10*, 521−526.
(10) Gui, Y.; Becker, C.; Dai, N.; Liu, J.; Qiu, Z.; Novik, E.; Schäfer, M.; Shu, X.; Chu, J.; Buhmann, H. Giant Spin-Orbit Splitting in a HgTe Quantum Well. *Phys. Rev. B: Condens. Matter Mater. Phys.* **2004**, *70*, 115328.
(11) Ying, J.-J.; Struzhkin, V. V.; Cao, Z.-Y.; Goncharov, A. F.; Mao, H.-K.; Chen, F.; Chen, X.-H.; Gavriliuk, A. G.; Chen, X.-J. Realization of Insulating State and Superconductivity in the Rashba Semiconductor BiTeCl. *Phys. Rev. B: Condens. Matter Mater. Phys.* **2016**, *93*, 100504.
(12) Akrap, A.; Teyssier, J.; Magrez, A.; Bugnon, P.; Berger, H.; Kuzmenko, A. B.; Van Der Marel, D. Optical Properties of BiTeBr and BiTeCl. *Phys. Rev. B: Condens. Matter Mater. Phys.* **2014**, *90*, 035201.
(13) Heid, R.; Bohnen, K. P.; Chis, V.; Volodin, V.; Kokh, K. A.; Tereshchenko, O. E.; Echenique, P. M.; Chulkov, E. V.; Sklyadneva, I. Y. Lattice Dynamics of Bismuth Tellurohalides. *Phys. Rev. B* **2012**, *86* (9), 094302−1−094302−8 2012.
(14) Jacimovic, J.; Mettan, X.; Pisoni, A.; Gaal, R.; Katrych, S.; Demko, L.; Akrap, A.; Forró, L.; Berger, H.; Bugnon, P. Enhanced Low-Temperature Thermoelectrical Properties of BiTeCl Grown by Topotactic Method. *Scr. Mater.* **2014**, *76*, 69−72.
(15) Zahid, F.; Lake, R. Thermoelectric Properties of Bi_2Te_3 Atomic Quintuple Thin Films. *Appl. Phys. Lett.* **2010**, *97*, 212102.
(16) Lee, H.-Y.; Chen, Y.-S.; Lin, Y.-C.; Wu, J.-K.; Lee, Y.-C.; Wu, B.-K.; Chern, M.-Y.; Liang, C.-T.; Chang, Y. H. Epitaxial Growth of Bi_2Te_3 Topological Insulator Thin Films by Temperature-Gradient Induced Physical Vapor Deposition (Pvd). *J. Alloys Compd.* **2016**, *686*, 989−997.
(17) Humlíček, J.; Hemzal, D.; Dubroka, A.; Caha, O.; Steiner, H.; Bauer, G.; Springholz, G. Raman and Interband Optical Spectra of Epitaxial Layers of the Topological Insulators Bi_2Te_3 and Bi_2Se_3 on BaF_2 Substrates. *Phys. Scr.* **2014**, *2014*, 014007.
(18) Shevelkov, A.; Dikarev, E.; Shpanchenko, R.; Popovkin, B. Crystal Structures of Bismuth Tellurohalides BiTeX (X= Cl, Br, I) from X-Ray Powder Diffraction Data. *J. Solid State Chem.* **1995**, *114*, 379−384.
(19) Chen, L.; Liu, B.; Ge, M.; Ma, Y.; Abbas, A. N.; Zhou, C. Step-Edge-Guided Nucleation and Growth of Aligned WSe_2 on Sapphire *via* a Layer-Over-Layer Growth Mode. *ACS Nano* **2015**, *9*, 8368−8375.
(20) Zhou, W.; Lu, J.; Xiang, G.; Ruan, S. Vibrational Properties of Layered BiTeCl Single Crystal. *J. Raman Spectrosc.* **2017**, *48*, 1783−1788.
(21) Kuiri, M.; Das, S.; Muthu, D.; Das, A.; Sood, A. Thickness Dependent Transition from the 1T′ to Weyl Semimetal Phase in Ultrathin $MoTe_2$: Electrical Transport, Noise and Raman Studies. *Nanoscale* **2020**, *12*, 8371−8378.
(22) Chen, B.; Sahin, H.; Suslu, A.; Ding, L.; Bertoni, M. I.; Peeters, F.; Tongay, S. Environmental Changes in $MoTe_2$ Excitonic Dynamics by Defects-Activated Molecular Interaction. *ACS Nano* **2015**, *9*, 5326−5332.
(23) Sahin, H.; Tongay, S.; Horzum, S.; Fan, W.; Zhou, J.; Li, J.; Wu, J.; Peeters, F. Anomalous Raman Spectra and Thickness-Dependent Electronic Properties of WSe_2. *Phys. Rev. B: Condens. Matter Mater. Phys.* **2013**, *87*, 165409.
(24) Cao, Y.; Sheremetyeva, N.; Liang, L.; Yuan, H.; Zhong, T.; Meunier, V.; Pan, M. Anomalous Vibrational Modes in Few Layer WTe_2 Revealed by Polarized Raman Scattering and First-Principles Calculations. *2D Mater.* **2017**, *4*, 035024.
(25) Li, Q.; Zhou, Q.; Shi, L.; Chen, Q.; Wang, J. Recent Advances in Oxidation and Degradation Mechanisms of Ultrathin 2D Materials under Ambient Conditions and Their Passivation Strategies. *J. Mater. Chem. A* **2019**, *7*, 4291−4312.
(26) Yang, S.; Cai, H.; Chen, B.; Ko, C.; Özçelik, V. O.; Ogletree, D. F.; White, C. E.; Shen, Y.; Tongay, S. Environmental Stability of 2D Anisotropic Tellurium Containing Nanomaterials: Anisotropic to Isotropic Transition. *Nanoscale* **2017**, *9*, 12288−12294.
(27) Yang, S.; Qin, Y.; Chen, B.; özçelik, V. O.; White, C. E.; Shen, Y.; Yang, S.; Tongay, S. Novel Surface Molecular Functionalization Route to Enhance Environmental Stability of Tellurium-Containing 2D Layers. *ACS Appl. Mater. Interfaces* **2017**, *9*, 44625−44631.
(28) Wang, X. H.; Yang, A. J.; Koratkar, N.; Chu, J. F.; Lv, P. L.; Rong, M. Z. Effects of Adatom and Gas Molecule Adsorption on the Physical Properties of Tellurene: A First Principles Investigation. *Phys. Chem. Chem. Phys.* **2018**, *20*, 4058−4066.
(29) Xu, W.; Gan, L.; Wang, R.; Wu, X.; Xu, H. Surface Adsorption and Vacancy in Tuning the Properties of Tellurene. *ACS Appl. Mater. Interfaces* **2020**, *12*, 19110−19115.
(30) Walia, S.; Sabri, Y.; Ahmed, T.; Field, M. R.; Ramanathan, R.; Arash, A.; Bhargava, S. K.; Sriram, S.; Bhaskaran, M.; Bansal, V. Defining the Role of Humidity in the Ambient Degradation of Few-Layer Black Phosphorus. *2D Mater.* **2017**, *4*, 015025.
(31) Gao, J.; Li, B.; Tan, J.; Chow, P.; Lu, T.-M.; Koratkar, N. Aging of Transition Metal Dichalcogenide Monolayers. *ACS Nano* **2016**, *10*, 2628−2635.
(32) Ahn, S.; Kim, G.; Nayak, P. K.; Yoon, S. I.; Lim, H.; Shin, H.-J.; Shin, H. S. Prevention of Transition Metal Dichalcogenide Photodegradation by Encapsulation with h-BN Layers. *ACS Nano* **2016**, *10*, 8973−8979.
(33) Fan, D.; Zhou, Q.; Lv, X.; Jing, J.; Ye, Z.; Shao, S.; Xie, J. Synthesis, Thermal Conductivity and Anti-Oxidation Properties of Copper Nanoparticles Encapsulated within Few-Layer h-BN. *Ceram. Int.* **2018**, *44*, 1205−1208.
(34) Papazoglou, A.; Rentzeperis, P. The Crystal Structure of Antimony Telluroiodide, SbTeI. *Zeitschrift für Kristallographie-Crystalline Materials* **1983**, *165*, 159−168.